Electronic Supplementary Material (ESI) for Journal of Materials Chemistry C.
This journal is © The Royal Society of Chemistry 2021

Regulating Metal Nodes of 1D Conjugated Coordination Polymers for Enhancing the Performance of Sodium-Ion Batteries

Kun Fan,[a] Chenyang Zhang,[a] Yuan Chen,[a] Guoqun Zhang,[a] Yanchao Wu,[a] Jincheng Zou[a] and Chengliang Wang[a]*

[a] School of Optical and Electronic Information, Wuhan National Laboratory for Optoelectronics (WNLO), Huazhong University of Science and Technology, Wuhan 430074, China. E-mail: clwang@hust.edu.cn

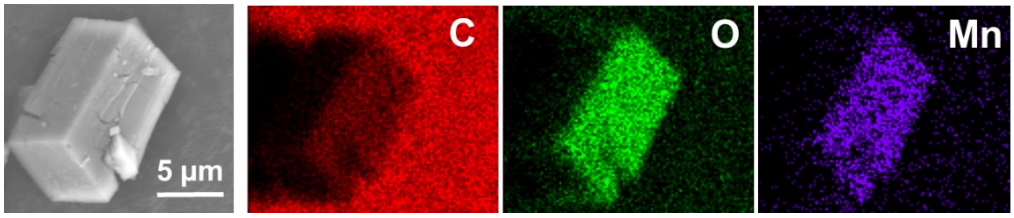

Figure S1. Energy dispersive X-ray spectrum (EDS-mapping) of **Mn-DHBQ**, indicating that the elements are evenly distributed in the material.

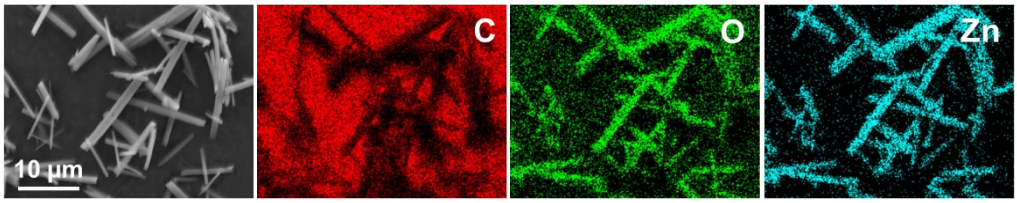

Figure S2. Energy dispersive X-ray spectrum (EDS-mapping) of **Zn-DHBQ**, indicating that the elements are evenly distributed in the material.

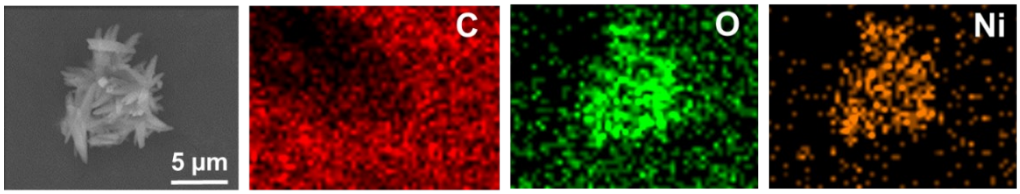

Figure S3. Energy dispersive X-ray spectrum (EDS-mapping) of **Ni-DHBQ**, indicating that the elements are evenly distributed in the material.

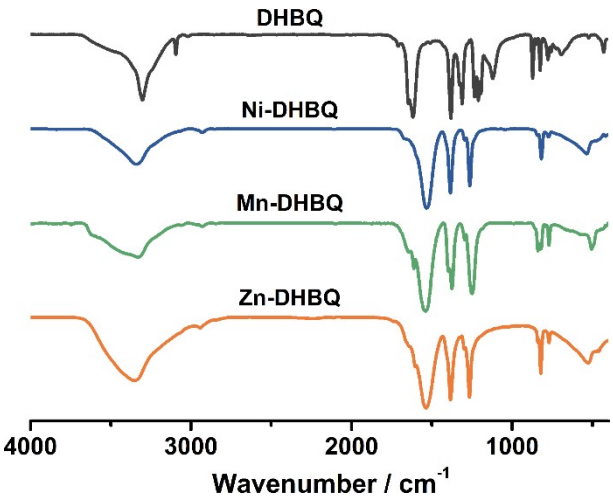

Figure S4. The FT-IR spectra of the free ligand and CCPs **M-DHBQ** (M=Ni, Mn, Zn).

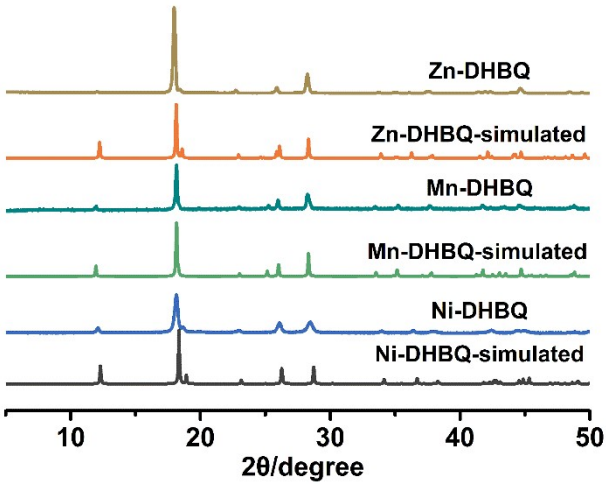

Figure S5. XRD patterns of **M-DHBQ** and the simulated XRD patterns by using the proposed crystal structures (CCDC 728411, 752734 and 752735 for **Mn-DHBQ**, **Zn-DHBQ** and **Ni-DHBQ**, respectively).

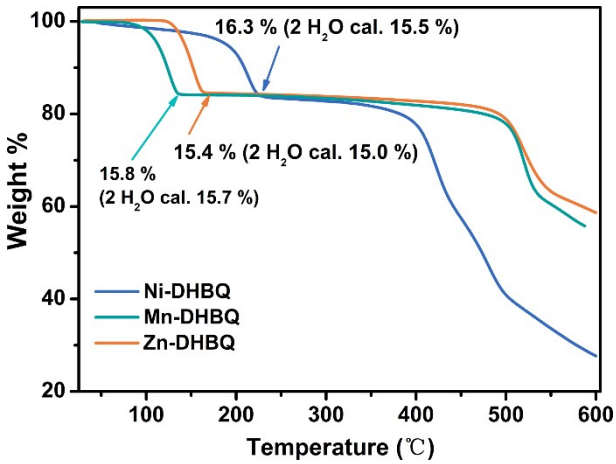

Figure S6. TGA curves of **M-DHBQ** (M=Ni, Mn, Zn).

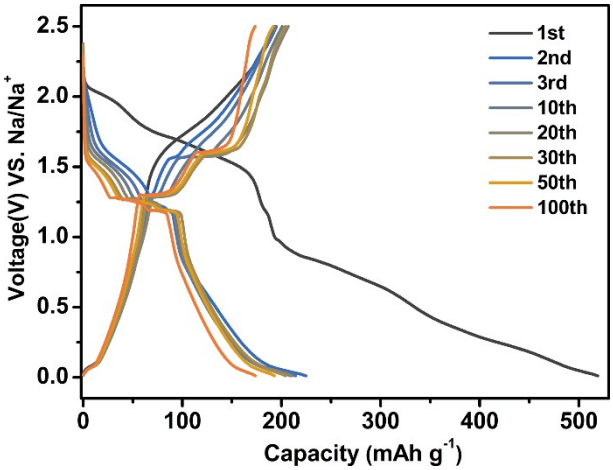

Figure S7. Discharge-charge voltage profiles of **Zn-DHBQ** at a current density of 0.1 A g^{-1}.

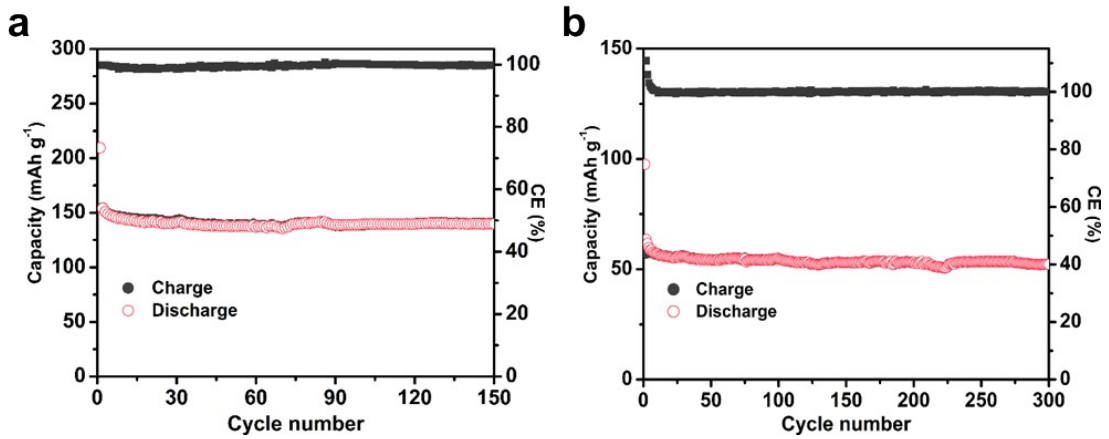

Figure S8. Cycling performance of super P at a rate of 0.1 A g^{-1} at the voltage ranges of (a) 0.01-2.5 V (vs. Na/Na^+) and (b) 0.5-2.3 V (vs. Na/Na^+), which showed reversible capacity of about 140 mAh g^{-1} and 53 mAh g^{-1}, respectively.

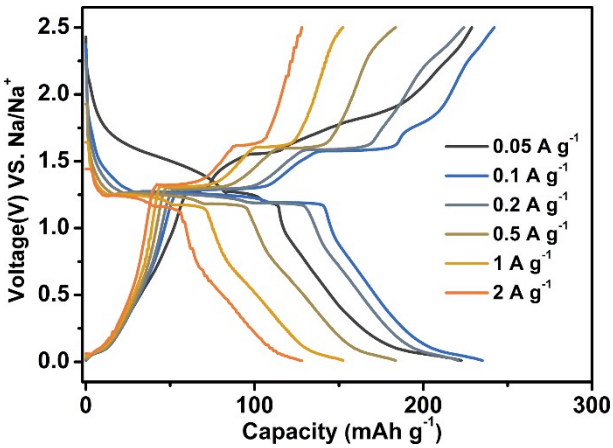

Figure S9. Discharge-charge voltage profiles of **Mn-DHBQ** at different current densities.

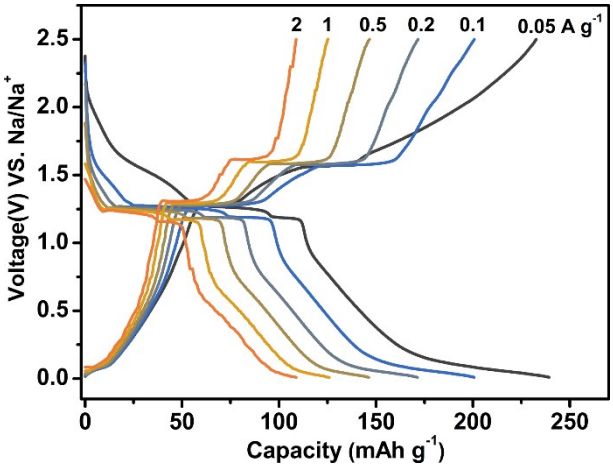

Figure S10. Charge-discharge profiles of **Zn-DHBQ** electrodes at different current densities.

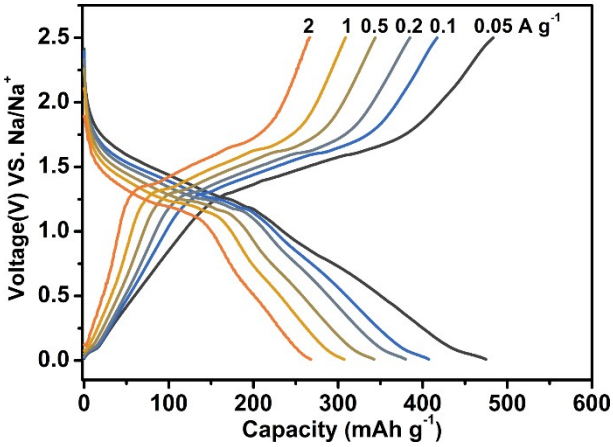

Figure S11. Charge-discharge profiles of **Ni-DHBQ** electrodes at different current densities.

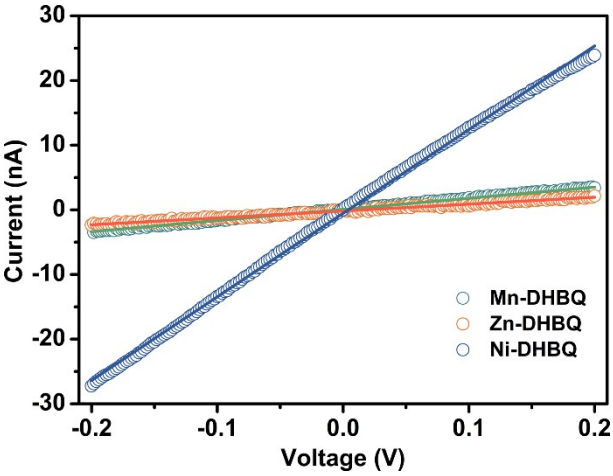

Figure S12. *I*-V curves for **M-DHBQ** (M= Mn, Zn and Ni). The electric conductivity of **Ni-DHBQ** was 3.8×10^{-7} S m^{-1}, which was higher than **Mn-DHBQ** (3.9×10^{-8} S m^{-1}) and **Zn-DHBQ** (3.1×10^{-8} S m^{-1}).

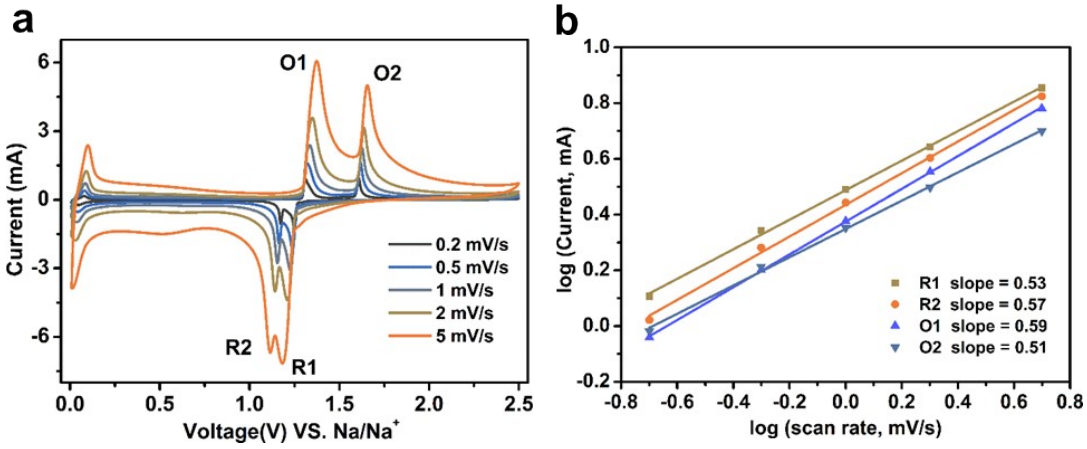

Figure S13. (a) CV curves of **Mn-DHBQ** electrode at different scan rates. (b) The corresponding plots of log(*i*) *vs.* log(*v*) for CV curves of **Mn-DHBQ** electrode at different scan rates.

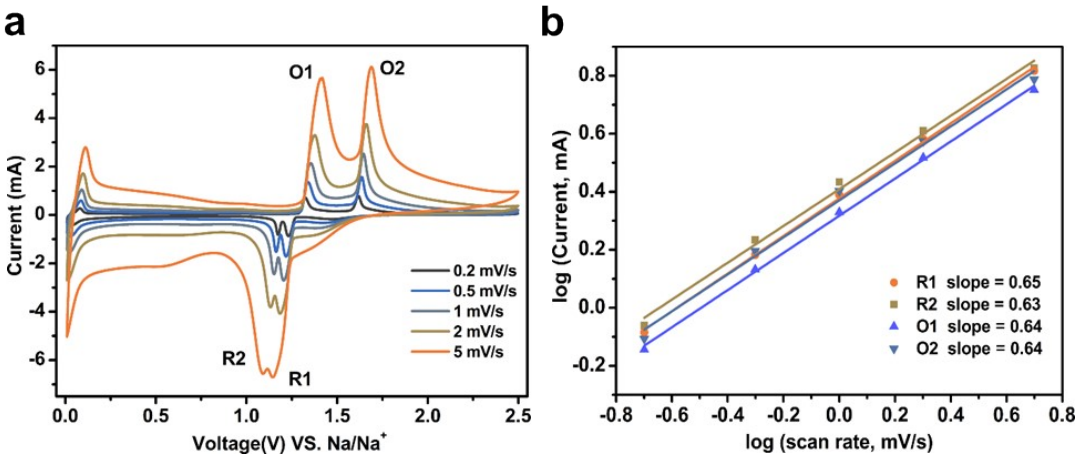

Figure S14. (a) CV curves of **Zn-DHBQ** electrode at different scan rates. (b) The corresponding plots of log(*i*) *vs.* log(*v*) for CV curves of **Zn-DHBQ** electrode at different scan rates.

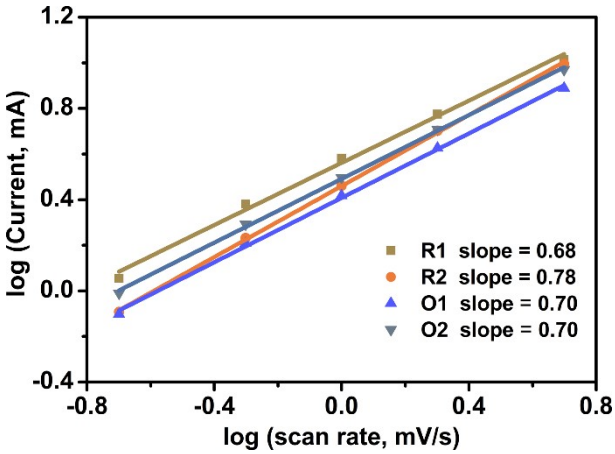

Figure S15. The corresponding plots of log(*i*) *vs.* log(*v*) for CV curves of **Ni-DHBQ** electrode at different scan rates.

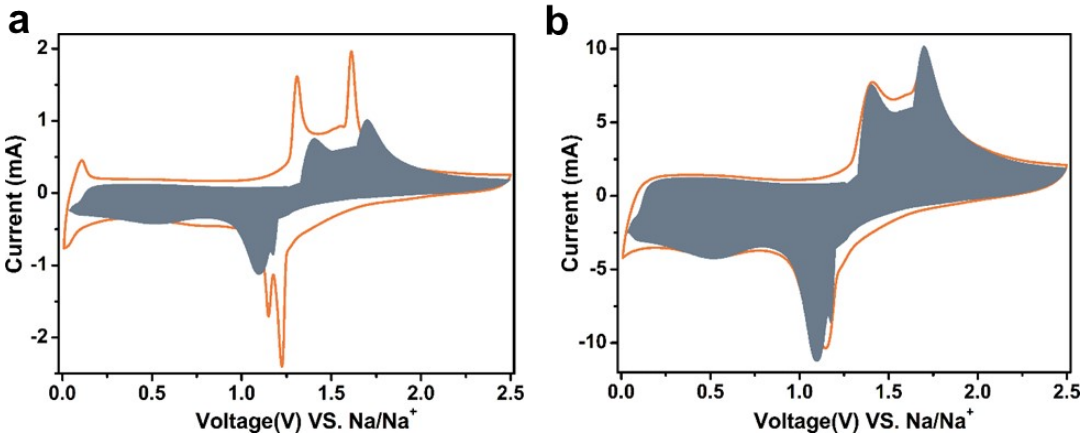

Figure S16. CV curves showing the capacitive contribution (the filled part) of the **Ni-DHBQ** at a scan rate of (a) 0.5, (b) 5 mV s^{-1}.

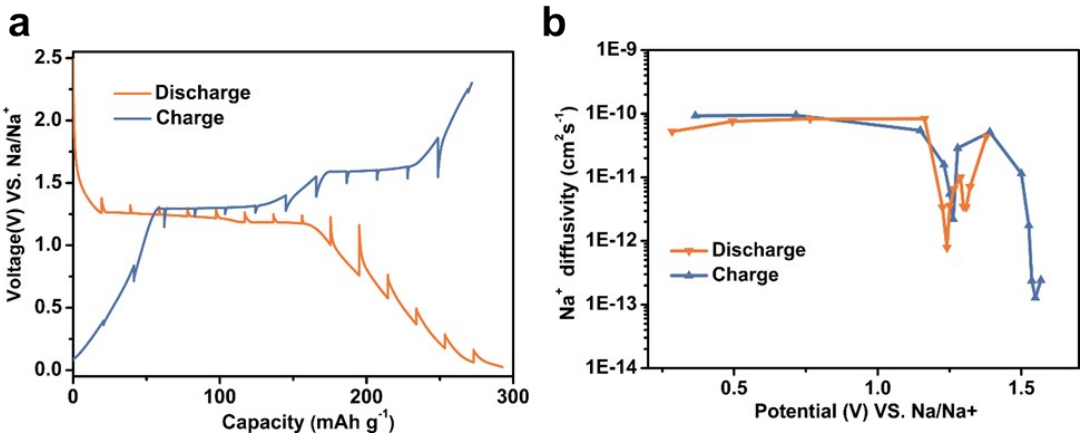

Figure S17. (a) GITT potential response curve with time. (b) The plot of Na-ion diffusivity calculated from GITT methods versus potential of **Mn-DHBQ** electrode.

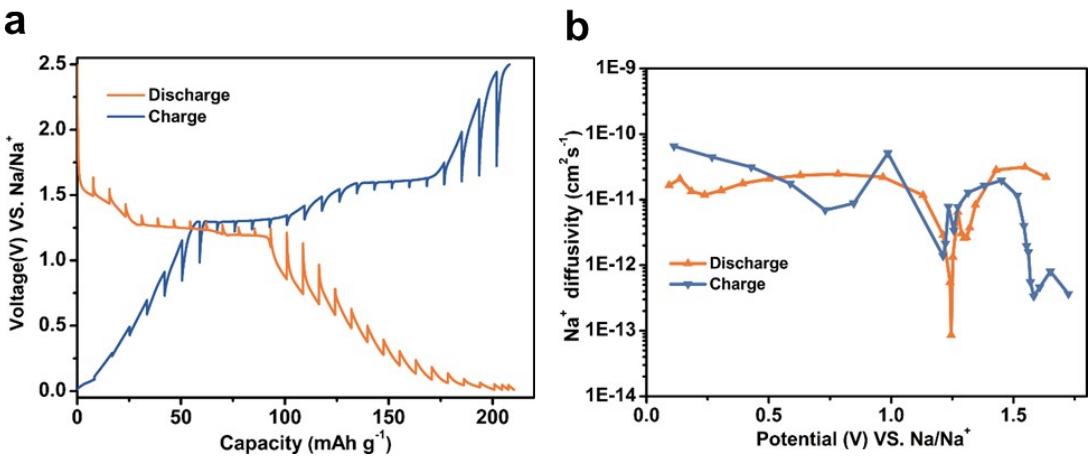

Figure S18. (a) GITT potential response curve with time. (b) The plot of Na-ion diffusivity calculated from GITT methods versus potential of **Zn-DHBQ** electrode.

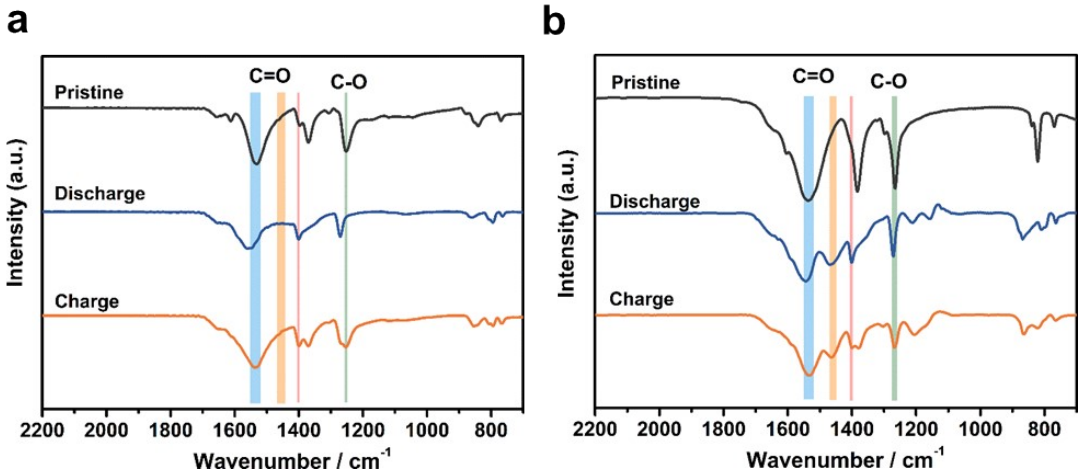

Figure S19. Ex-situ FT-IR spectra of (a) **Mn-DHBQ** and (b) **Zn-DHBQ** electrode recorded at different potentials.

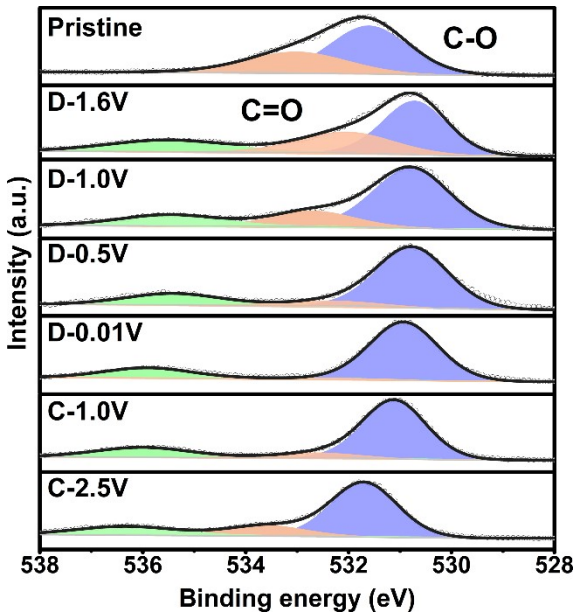

Figure S20. Ex-situ XPS O 1s spectra of **Ni-DHBQ**.

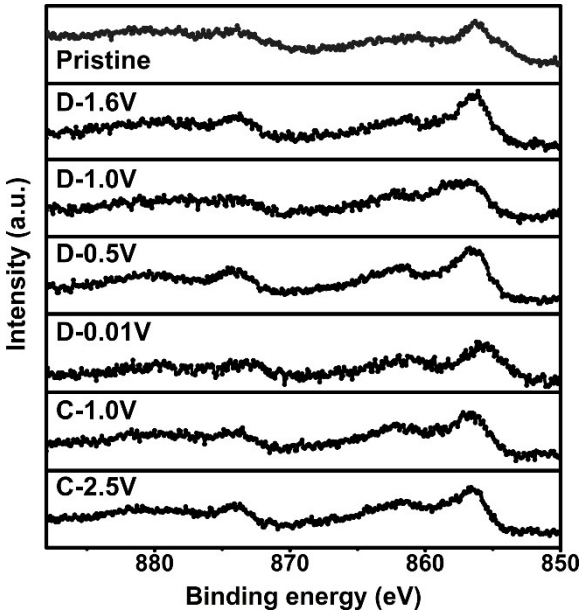

Figure S21. Ex-situ XPS Ni 2p spectra of **Ni-DHBQ**.

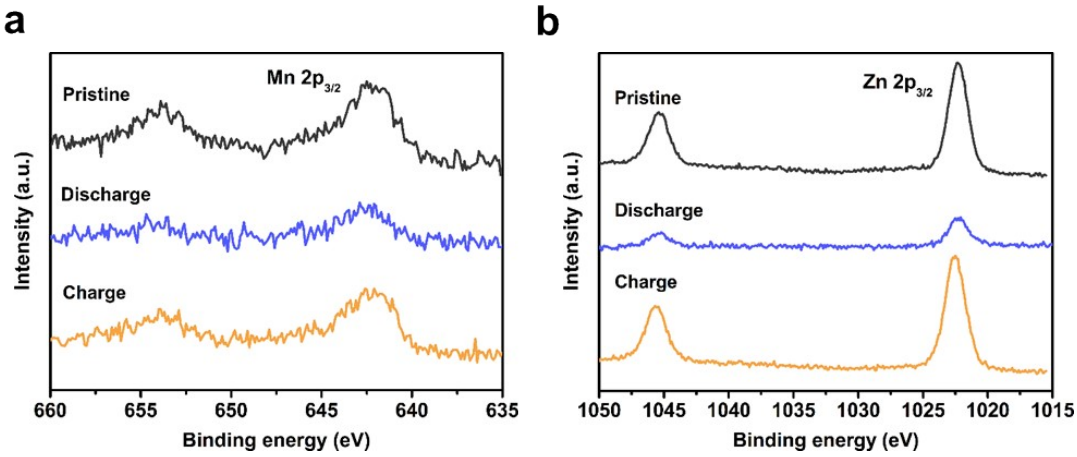

Figure S22. (a) Ex-situ XPS Mn 2p spectra of **Mn-DHBQ**. (b) Ex-situ XPS Zn 2p spectra of **Zn-DHBQ**.

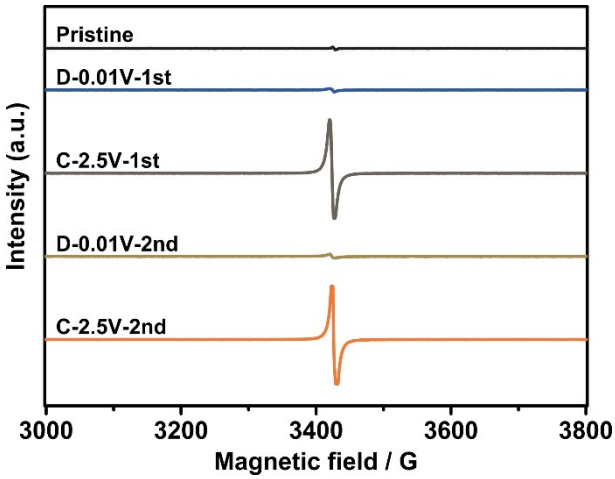

Figure S23. Ex-situ EPR spectra of **Zn-DHBQ** electrode recorded at different potentials during the first and second cycle.

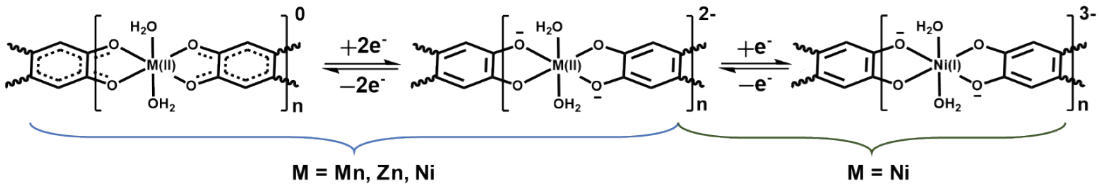

Figure S24. Possible charge storage mechanism of **M-DHBQ**.

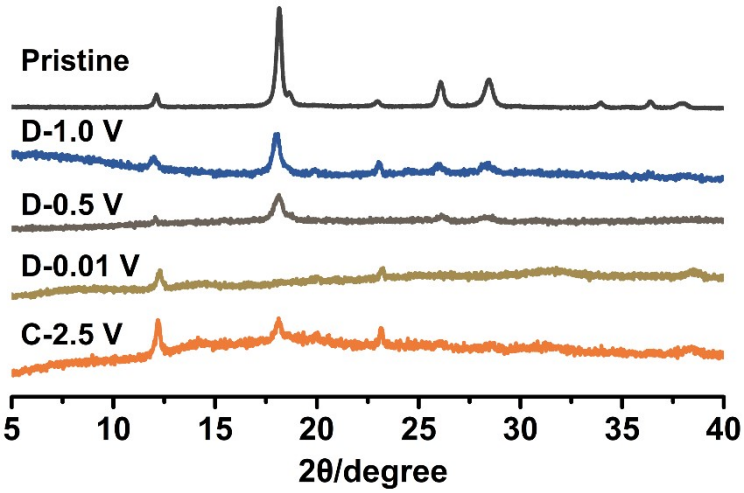

Figure S25. *E*x-situ PXRD of **Ni-DHBQ** electrode recorded at different potentials.

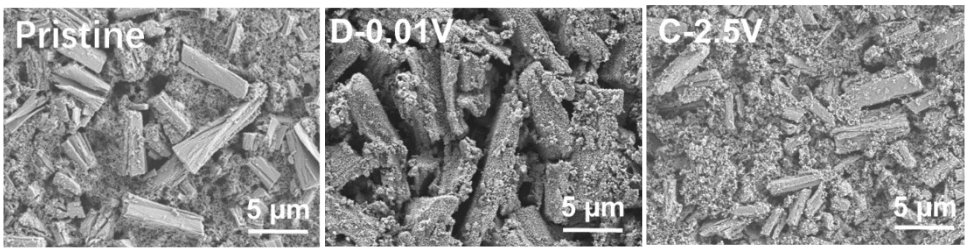

Figure S26. SEM images of the **Zn-DHBQ** electrode recorded at different potentials.

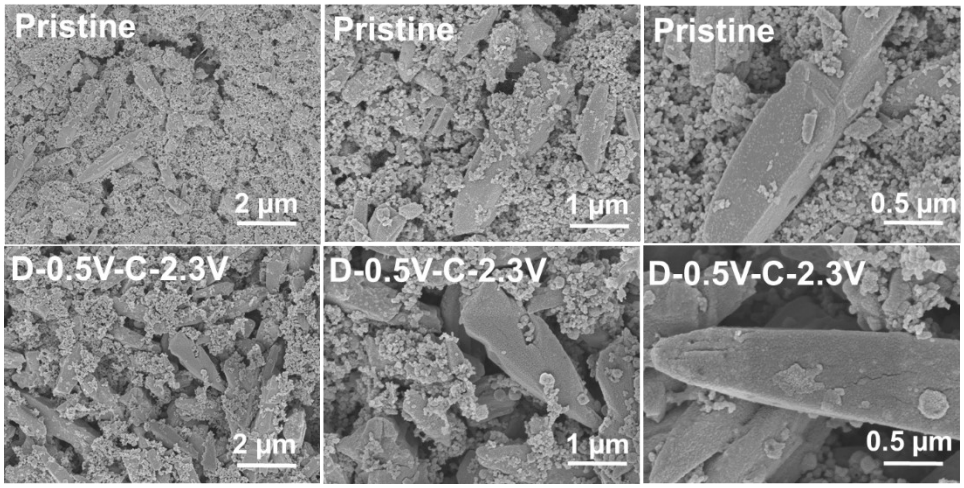

Figure S27. SEM images of the **Ni-DHBQ** electrode recorded at 2.3 V. The **Ni-DHBQ** electrode was first discharge to 0.5 V and then charge to 2.3 V. The particle size kept stable after cycling.

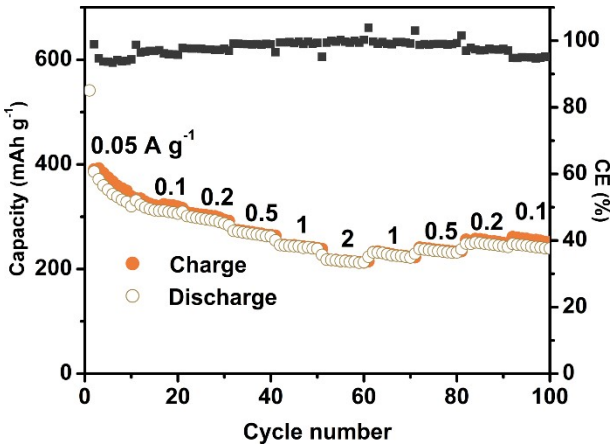

Figure S28. Rate capability of the **Ni-DHBQ** in the 0.5-2.3 V range.

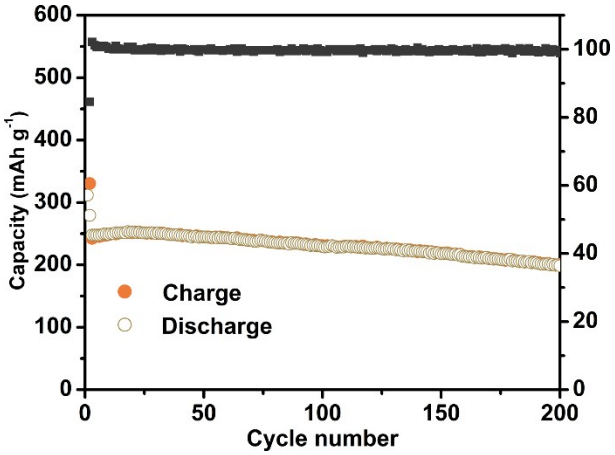

Figure S29. Cycling performance of **Ni-DHBQ** electrodes at a current density of 1 A g^{-1} in the 0.5-2.3 V range.

Table S1. Electrochemical performance of DHBQ-based electrode materials for SIBs.

Type	Electrode	Operation voltage window (V)	Low-rate capacity (mAh g^{-1}) (Current (mA g^{-1}))	High-rate capacity (mAh g^{-1}) (Current (mA g^{-1}))	Reversible capacity (mAh g^{-1}) (Current (mA g^{-1}), cycle number)	Ref.
Small Molecule	DHBQDS (Na_2DHBQ)	0.8-2.5	290 (20)	68 (1000)	167 (200, 300)	1
	Na_2DHBQ	1.0-2.0	265 (29)	/	/	2
	Na_2DHBQ	1.0-2.0	288 (29)	/	40 (29, 10)	3
	Na_2DHBQ/CNT	1.0-2.0	259 (29)	142 (2030)	191 (290, 30)	
	Na_2DHBQ	0.5-2.5	265 (29.1)	159 (1455)	231 (29.1, 50) 181 (291, 300)	4
Organic Polymer	Na_2PDS ($Na_2PDHBQS$)	0.01-3	224.9 (100)	131 (1000)	183 (100, 150) 138 (500, 500)	5
	$Na_2PDHBQS$	0.8-2.2	123 (100)	83 (1000)	121 (100, 150)	6
	$Na_2PDHBQS$/RGO	0.8-2.2	179 (100)	147 (1000)	183 (100, 150) 110 (1000, 500)	
CCPs	**Mn-DHBQ**	0.01-2.5	261 (100)	129 (2000)	230 (100,150) 112 (1000, 500)	**This work**
	Zn-DHBQ	0.01-2.5	212 (100)	109 (2000)	167 (100,150) 93 (1000, 500)	**This work**
	Ni-DHBQ	0.01-2.5	424 (100)	267 (2000)	321 (100,150) 243 (1000, 500)	**This work**
		0.5-2.3	320 (100)	215 (2000)	215 (100, 150) 140 (5000, 500)	**This work**

References

1 C. Luo, J. Wang, X. Fan, Y. Zhu, F. Han, L. Suo and C. Wang, *Nano Energy* 2015, **13**, 537-545.

2 X. Wu, S. Jin, Z. Zhang, L. Jiang, L. Mu, Y. S. Hu, H. Li, X. Chen, M. Armand, L. Chen and X. Huang, *Sci Adv* 2015, **1**, e1500330.

3 X. Wu, J. Ma, Q. Ma, S. Xu, Y.-S. Hu, Y. Sun, H. Li, L. Chen and X. Huang, *J. Mater. Chem. A* 2015, **3**, 13193-13197.

4 Z. Zhu, H. Li, J. Liang, Z. Tao and J. Chen, *Chem. Commun.* 2015, **51**, 1446-1448.

5 D. Wu, Y. Huang and X. Hu, *Chem. Commun.* 2016, **52**, 11207-11210.

6 A. Li, Z. Feng, Y. Sun, L. Shang and L. Xu, *J. Power Sources* 2017, **343**, 424-430.